HHS Public Access

Author manuscript

J Cutan Pathol. Author manuscript; available in PMC 2021 January 01.

Published in final edited form as:

J Cutan Pathol. 2021 January ; 48(1): 53–65. doi:10.1111/cup.13871.

Angulated small nests and cords: key diagnostic histologic features of infiltrative basal cell carcinoma can be identified using integrated reflectance confocal microscopy-optical coherence tomography

Melissa Gill, MD[*,1,2,3], Aditi Sahu, PhD[*,4], Christi Alessi-Fox, MS[5], Miguel Cordova, MD[4], Salvador Gonzalez, MD, PhD[3], Nicusor Iftimia, PhD[6], Saud Aleissa, MD[4], Cristian Navarrete-Dechent, MD[4,✣], Stephen Dusza, DrPH[4], Anthony Rossi, MD[4], Ashfaq A. Marghoob, MD[4], Milind Rajadhyaksha, PhD[,4], Chih-Shan J. Chen, MD, PhD[**,4]**

[1]Department of Pathology, SUNY Downstate Medical Center, Brooklyn, NY, USA

[2]SkinMedical Research and Diagnostics, P.L.L.C., Dobbs Ferry, NY, USA

[3]Faculty of Medicine and Health Sciences, University of Alcala de Henares, Madrid, Spain

[4]Dermatology Service, Department of Medicine, Memorial Sloan Kettering Cancer Center, New York, NY; USA

[5]Caliber Imaging and Diagnostics Inc., 50 Methodist Hill Drive Suite 1000, Rochester, NY

[6]Physical Sciences, Inc., 20 New England Business Ctr. Drive, Andover, MA

Abstract

Background—Accurate basal cell carcinoma (BCC) subtyping is requisite for appropriate management, but non-representative sampling occurs in 18–25% of biopsies. By enabling non-invasive diagnosis and more comprehensive sampling, integrated reflectance confocal microscopy-optical coherence tomography (RCM-OCT) may improve accuracy of BCC subtyping and subsequent management. We evaluated RCM-OCT images and histopathology slides for the presence of two key features, angulation and small nests and cords, and calculated (i) sensitivity and specificity of these features, combined and individually, for identifying an infiltrative BCC subtype and (ii) agreement across modalities.

Methods—Thirty-three RCM-OCT imaged, histopathology-proven BCCs (17 superficial and/or nodular; 16 containing an infiltrative component) were evaluated.

Corresponding author: Melissa Gill, MD: mgill@skinmedicalranddx.com.

✣This author performed this work while at Memorial Sloan Kettering Cancer Center, but is now affiliated with Department of Dermatology, Pontificia Universidad Católica de Chile, Santiago, Chile

*Melissa Gill and Aditi Sahu contributed equally to this work and should be considered joint first author.

**Milind Rajadhyaksha and Chih-Shan J. Chen contributed equally to this work and should be considered joint senior author.

Authorship Contributions:

(1) Acquisition, analysis and interpretation of data. MG, AS, CMAF, MC, SA, SG, CN-D, AR, C-SJC, NI, MR.

(2) Drafting and revising the article. MG, AS, SA, CMAF, SG, MR, C-SJC.

(3) Final approval of the version to be published. MG, AS, CMAF, MC, SG, NI, SA, CN-D, SD, AR, AAM, MR, SG, C-SJC.

Results—The presence of *angulation* or *small nests and cords* was sufficient to identify infiltrative BCC on RCM-OCT with 100% sensitivity and 82% specificity, similar to histopathology (100% sensitivity, 88% specificity, kappa=0.82). When both features present, the sensitivity for identifying infiltrative BCC was 100% using either modality and specificity was 88% on RCM-OCT versus 94% on histopathology, indicating near perfect agreement between non-invasive and invasive diagnostic modalities (kappa=0.94).

Conclusions—RCM-OCT can non-invasively identify key histopathologic features of infiltrative BCC offering a possible alternative to traditional invasive biopsy. Further studies are necessary.

Keywords

basal cell carcinoma; in vivo diagnosis; reflectance confocal microscopy; optical coherence tomography; histopathology

Introduction

Appropriate management of BCC depends on histopathologic subtyping into the following categories: superficial, nodular and high risk.[1–3] A high risk subtype is present in 30–40% of BCCs and frequently represents part of a mixed pattern.[4–8] As up to 54% of BCCs show a mixed pattern, partial biopsies may "under-call" a high risk subtype, leading to mismanagement, with potentially devastating results.[1,5,7,9] Non-invasive imaging tools may enable representative sampling without excisional biopsy.

Reflectance confocal microscopy (RCM) and optical coherence tomography (OCT) are complementary non-invasive skin imaging modalities based on backscattering of light. RCM produces high resolution (~1 μm) images enabling visualization of cytomorphology and architecture to a maximum depth of ~0.20 mm (papillary dermis). Mosaicking or consecutive depth-stacking of images allows for a volumetric RCM field of view (FOV) up to 8 mm × 8 mm × 0.20 mm. By contrast, OCT produces moderate resolution (~10 μm) images enabling visualization of architecture to a maximum depth of ~ 1 mm (reticular dermis), and rastering allows for a volumetric FOV up to 6 mm × 6 mm × 1 mm.

Specific structures seen in BCC on histopathology can be identified using both RCM and OCT.[10–16] Several groups have reported that in vivo diagnosis of BCC is achievable with high sensitivity and specificity using RCM;[17–21] whereas due to its relatively lower resolution, OCT lacks diagnostic specificity as a stand-alone tool.[22–25] However, OCT can reliably distinguish normal skin from tumor; therefore, with its larger field of view, OCT enables more comprehensive assessment of tumor depth and/or margins.[22,24–28] We have previously shown that a handheld integrated (originally called combined) RCM-OCT device with the RCM FOV captured in center of the co-registered OCT FOV (Figure 1) allows for more accurate BCC diagnosis as the operator can see the tumor at cellular-level resolution while, in the same location, assessing the lesion's depth and 3-dimensional (3D) architecture.[25,29] By moving this handheld device over the skin, integrated RCM-OCT allows for examination of all or most of a BCC's volume in real-time, enabling non-invasive diagnosis and triage at the bedside.[25] However, for effective triage and management, accurate subtyping is also crucial.

RCM[20,30,31] and OCT[14,15,32] have shown feasibility for BCC subtyping. One study using excision histopathology as the gold standard found that in vivo RCM was slightly superior at subtyping than punch biopsy in the hands of an expert.[20] However, prior studies have often used non-specific or new terminology, making widespread adoption and accurate application of subtyping criteria more difficult. Adopting standard histopathology criteria, when applicable, offers an as yet under-utilized but practical approach to mitigate such challenges.

The goal of this study was to ascertain whether specific histopathologic terminology used to diagnose high risk BCCs could be applied directly to RCM and OCT. Of the high risk subtypes, infiltrative is the most common and morpheaform is the second most common, representing 55% and 23% of high risk BCCs, respectively.[8] On histopathology, infiltrative and morpheaform BCC both characteristically contain intradermal tumor aggregates with angulated contours arranged as nests (often small in size) and/or cords.[1,2,4,6,7] Thus, the aims were to 1) determine whether (i) "*angulation*" and/or (ii) arrangement in "*small nests" and/or "cords"* can be identified in dermal BCC tumor aggregates by RCM and/or OCT using the handheld integrated RCM-OCT device, 2) assess whether the presence of these features, either combined or individually, are sensitive or specific for the identification of an infiltrative subtype, and 3) compare whether the presence or absence of these features on RCM or OCT correlates with their presence or absence on histopathology across BCC subtypes.

Materials and Methods

Study type

This was a retrospective observational study.

Case selection

One hundred and thirty BCCs were collected through a prospective IRB-approved study conducted between March 2017 and July 2019 at Memorial Sloan Kettering Cancer Center. All patients gave written informed consent prior to imaging. Lesions which were clinically or dermoscopically suspicious for BCC and underwent biopsy or excision subsequent to imaging were included in this study. Lesions not accessible with the RCM-OCT device due to anatomical location (e.g. inside the ear) or which were previously biopsied were excluded. All histopathology specimens were diagnosed and subtyped by a board-certified dermatopathologist. From this dataset, all BCCs which contained an infiltrative subtype on histopathologic diagnosis (mixed or pure) and an equal number of randomly selected controls without an infiltrative pattern on histopathology were included for this retrospective study. Due to the limited size of the dataset, age-, gender- and site-matching of controls was not feasible and therefore not performed. Patient age, patient sex, tumor location, histopathology specimen type(s), and histopathologic diagnosis with subtype(s) were recorded.

Integrated reflectance confocal microscopy-optical coherence tomography device and imaging protocol

Images were captured using the integrated RCM-OCT prototype (developed by Physical Sciences, Inc., Andover, MA, in collaboration with Caliber Imaging & Diagnostics, Inc., Rochester, NY). This currently unique integrated prototype, which is not yet commercially available, represents the only device that allows simultaneous, spatially co-registered real-time RCM and OCT imaging using the same probe. Imaging was guided by dermoscopy and performed in quadrants as previously described.[33–35] For each suspicious area, one RCM stack (FOV: 0.75 mm × 0.75 × 0.20 mm deep) centered in the corresponding OCT raster (FOV: 2 mm × 2 mm × 1 mm deep) were simultaneously acquired (Figure 1). Comprehensive 3D OCT sampling (analogous to excisional biopsy) of each BCC was attempted by imaging multiple (2–7) adjacent sites with contiguous OCT FOVs.

Feature Analysis

All captured RCM and OCT images from all RCM-OCT image sets and all available histopathology slides were retrospectively evaluated by a board-certified dermatopathologist for the presence of the following features within dermal tumor aggregates: (i) *angulation* and (ii) arrangement in “*small nests” and/or “cords.”* For each case, all RCM-OCT image sets were reviewed prior to histopathology slides. For each individual RCM-OCT image set, the RCM image stack was reviewed prior to the OCT raster. Figure 2 provides descriptions of each feature with examples across modalities. The feature evaluator was aware that all lesions were BCCs, but was blinded to the original histopathology reports containing the diagnostic subtyping.

Outcomes and statistical analysis

The primary outcome was identification of (i) *angulation* and/or (ii) “*small nests” and “cords”* in BCCs by RCM and/or OCT. The secondary outcome was sensitivity and specificity (with corresponding 95% confidence interval) of these features, combined and individually, for identifying the presence of an infiltrative BCC subtype using histopathologic diagnosis with subtyping as the gold standard. A tertiary outcome was the agreement (kappa) of feature identification between RCM, OCT and histopathology within the same tumor.

Results

Thirty-three BCCs from 22 patients were included. Per histopathologic diagnosis, 16 BCCs from 13 patients (mean age 73 years; 50% male; 88% on head/neck, 6% on trunk) harbored an infiltrative subtype, one pure and 15 mixed patterns (2 superficial-nodulo-infiltrative; 13 nodulo-infiltrative), satisfying inclusion criteria. Seventeen non-high risk BCC controls from 10 patients (mean age 58 years; 69% male; 29% on head/neck, 47% on trunk) consisted of 4 purely superficial, 10 purely nodular and 3 mixed superficial and nodular patterns. Patient and tumor characteristics are shown in Table 1.

Integrated RCM-OCT enabled non-invasive identification of both *angulation* and *small nests and/or cords* in the dermal component of BCCs with near perfect agreement with histopathology (Table 2, Table 3, Table 4). The simultaneous presence of *angulation* and *small nests and/or cords* correlated with the diagnostic presence of an infiltrative BCC subtype almost as well on integrated RCM-OCT as with histopathology (kappa=0.94). Both identified these features in 16/16 (100% sensitivity) infiltrative BCCs (Figure 3, Figure 4, Figure 5, Figure 6). These features were seen in one non-high risk BCC on both histopathology (1/17, 94% specificity) and RCM-OCT and in a second by RCM-OCT only (2/17, 88% specificity). The shared “false positive” showed a focal central superficial area mimicking infiltrative BCC within a well-circumscribed nodular pattern. This area was identified on OCT but not on RCM as it was outside the RCM FOV. The other “false positive” case on RCM-OCT was also positive only on OCT. Upon review, the structures in this case which resembled angulated nests and cords on OCT surround a well-defined tumor nodule and probably correspond to peritumoral areas on histopathology showing fibrosis with thickened collagen bundles, an increased number of small blood vessels and inflammation. Because exhaustive sectioning was not performed, “false negative” histopathology cannot be unequivocally excluded.

As stand-alone features, *angulation* and *small nests and/or cords* each showed high accuracy with 100% sensitivity for identifying an infiltrative BCC component on both integrated RCM-OCT and histopathology (Table 2, Table 3, Table 4). *Angulation* alone was present in 2/17 non-high risk BCCs on RCM-OCT (88% specificity) and only 1/17 by histopathology (94% specificity) as described above. *Small nests and/or cords* were identified in an additional non-high risk BCC by both RCM-OCT (3/17, 82% specificity) and histopathology (2/17, 88% specificity), but these did not represent overlapping cases. Near perfect agreement was also achieved between histopathology and RCM-OCT for the presence of *angulation* (kappa=0.94) and *small nests and/or cords* (kappa=0.82).

When examining the performance of each modality separately, OCT and histopathology performed similarly, both showing very good specificity and 100% sensitivity, while RCM showed slightly higher specificity but significantly lower sensitivity (Table 2, Table 3, Table 4). For each modality, the presence of both *angulation* and *small nests and/or cords* was most specific but only RCM reached 100% specificity. As a stand-alone feature, *angulation* was slightly more specific than *small nests and/or cords* across modalities. However, on RCM, while identifying angulation showed 100% specificity for the presence of an infiltrative BCC pattern, it showed only 56% sensitivity.

Discussion

In this study, identifying both (i) *angulation* and (ii) arrangement in *small nests and/or cords* within intradermal BCC tumor aggregates correlated with the presence of an infiltrative subtype with similar accuracy (kappa=0.94) using integrated RCM-OCT imaging (100% sensitive, 88% specific) as with histopathology (100% sensitive, 94% specific), implying that non-invasive diagnosis using integrated RCM-OCT may be both feasible and reliable using standard histopathology diagnostic terminology and criteria. Previous studies have also shown good correlation between histopathologic features and RCM features,[11,12,16,36–38] suggesting it is reasonable to apply diagnostic terms and criteria used in dermatopathology when examining a lesion by RCM-OCT. These findings are important as apprehension regarding the commitment to learn a new skill is common, and barriers to adoption of non-invasive technologies include the perceived need to learn new diagnostic terminology and criteria. If vetted histopathology features could be applied to RCM and OCT, some adoption barriers may be alleviated.

It is interesting that *angulation* and *small nests and/or cords* performed well individually on both integrated RCM-OCT (100% sensitivity and 88% versus 82% specificity, respectively) and histopathology (100% sensitivity and 94% versus 88% specificity, respectively). While concordance between integrated RCM-OCT and histopathology was not perfect on a case by case basis, given the differing sampling methods, it is not surprising that some variance was identified. Considering the limited sampling by RCM using the study protocol and the significantly lower resolution of OCT, agreement with histopathology was excellent.

Although OCT alone performed as well as combined RCM-OCT in identifying an infiltrative BCC subtype, OCT lacks the cellular level resolution provided by RCM which is needed to establish a diagnosis *in vivo*. The imaging protocol was designed to ensure comprehensive sampling by OCT only. For every 4 mm^3 volume of tumor imaged by OCT, only 0.1125 mm^3 was imaged by RCM (Figure 1). Therefore, it is not surprising that RCM alone showed lower sensitivity. Using histopathologic diagnosis of excision specimens as the gold standard, punch biopsy was previously shown to be slightly inferior for diagnosis and high risk BCC subtype detection as compared to expert interpretation of RCM images, which were captured across the entire lesional surface area (mimicking a broad shave "removal").[20] In the aforementioned study, concordance between punch biopsy and excision specimen for BCC diagnosis and subtyping was 75%, similar to prior studies.[4,7] If we altered our imaging protocol to acquire contiguous RCM FOVs (with overlapping OCT FOVs), the sensitivity of RCM would likely increase, mimicking those of the study above. However, such a protocol would increase imaging time without necessarily improving results as our study suggests OCT (if available) is sufficient for subtype detection once RCM has established a BCC diagnosis. While our cohorts are too small to draw a definitive conclusion, it is noteworthy that our integrated RCM-OCT protocol seems to perform better than shave or punch biopsies, a quarter of which miss high risk patterns.[4,5,20] Non-invasive BCC diagnosis and subtyping could be especially impactful on cosmetically sensitive areas, such as the nose, where biopsy more frequently misses more high risk subtypes (probably due to physician hesitance to perform a more scarring biopsy), and delay in diagnosis is more likely to result in disfiguring, complicated and/or expensive surgery.[5]

In conclusion, our results (i) suggest that integrated RCM-OCT shows promise as a reasonable alternative to histopathology for identifying an infiltrative BCC component and (ii) support prior studies which reported that specific structures seen in BCC on histopathology can be identified on both RCM and OCT, implying that histopathology terminology could be applied in these settings. Interestingly, our results also suggest that, after a diagnosis of BCC has been established, finding either *angulation* or arrangement in *small nests and/or cords* within dermal tumor aggregates on either RCM or OCT is quite specific for the presence of an infiltrative component. This is exciting as it could potentially (i) allow for better inter and intra-observer subtyping agreement and/or (ii) increase diagnostic confidence in settings where a reader identifies both features or is unsure about the presence of one feature but sees clear evidence of the other.

The limitations of this study include: small sample size; controls which are not age-, gender- and site-matched; limited sampling with RCM relative to more comprehensive sampling that is possible; its retrospective and descriptive nature; and that, while RCM and OCT images were reviewed separately from and prior to histopathology, the RCM and OCT image sets were provided together and not randomized and independently blinded. It is also unclear whether dermatopathologists and Mohs micrographic surgeons, who are accustomed to recognizing and applying standard histopathologic diagnostic features, may identify *angulation* and/or *small nests and/or cords* on RCM or OCT with more ease. Larger blinded prospective studies using readers with varying background experience (dermatopathologists, Mohs micrographic surgeons, dermatologists) are needed to confirm the findings in this study and determine whether these features are deployable across specialties.

Acknowledgements

The authors would like to thank Nicole Dimnet for administrative assistance with formatting and editing.

Funding source: This study was supported by NIH/NIBIB grant R01EB020029 and by MSKCC's NIH/NCI grant P30CA008748.

Conflicts of interest: Melissa Gill is a consulting investigator on an investigator-initiated study for DBV technologies on a topic unrelated to those described in this study and serves as a research consultant to the Dermatology Service, Department of Medicine, Memorial Sloan Kettering Cancer Center, New York, NY, USA. Christi Alessi-Fox is employed by and owns equity in Caliber Imaging and Diagnostics, Inc. (formerly Lucid, Inc), the company that manufactures and sells the VivaScope confocal microscope. N. Iftimia reports a patent (US9655521 B2) that is assigned to Physical Sciences Inc. (PSI) and Memorial Sloan Kettering Cancer Center (MSKCC), which is related to the technology Described in this study. PSI is the company that manufactured the instrument. Milind Rajadhyaksha is a former employee of and owns equity in Caliber Imaging and Diagnostics (formerly Lucid Inc.). The VivaScope is the commercial version of an original laboratory prototype that he developed at Massachusetts General Hospital, Harvard Medical School. Chih-Shan J. Chen is the principal investigator of unrelated studies sponsored by Apollo Medical Optics, Inc. This research was completed without financial support from either or Caliber I.D. or PSI, and data were acquired and processed from patients by coauthors unaffiliated with any commercial entity.

References

1. Sexton M, Jones DB, Maloney ME. Histologic pattern analysis of basal cell carcinoma. Study of a series of 1039 consecutive neoplasms. J Am Acad Dermatol. 1990;23(6 Pt 1):1118–1126. [PubMed: 2273112]
2. McKenzie CA, Chen AC, Choy B, Fernandez-Penas P, Damian DL, Scolyer RA. Classification of high risk basal cell carcinoma subtypes: experience of the ONTRAC study with proposed definitions and guidelines for pathological reporting. Pathology. 2016;48(5):395–397. [PubMed: 27311865]
3. Nehal KS, Bichakjian CK. Update on Keratinocyte Carcinomas. N Engl J Med. 2018;379(4):363–374. [PubMed: 30044931]
4. Russell EB, Carrington PR, Smoller BR. Basal cell carcinoma: a comparison of shave biopsy versus punch biopsy techniques in subtype diagnosis. J Am Acad Dermatol. 1999;41(1):69–71. [PubMed: 10411414]
5. Cohen PR, Schulze KE, Nelson BR. Basal cell carcinoma with mixed histology: a possible pathogenesis for recurrent skin cancer. Dermatol Surg. 2006;32(4):542–551. [PubMed: 16681663]
6. Crowson AN. Basal cell carcinoma: biology, morphology and clinical implications. Mod Pathol 2006;19 Suppl 2:S127–147. [PubMed: 16446711]

7. Haws AL, Rojano R, Tahan SR, Phung TL. Accuracy of biopsy sampling for subtyping basal cell carcinoma. J Am Acad Dermatol. 2012;66(1):106–111. [PubMed: 21798620]

8. Nedved D, Tonkovic-Capin V, Hunt E, et al. Diagnostic concordance rates in the subtyping of basal cell carcinoma by different dermatopathologists. J Cutan Pathol. 2014;41(1):9–13. [PubMed: 24152016]

9. van Delft LCJ, Nelemans PJ, Abdul Hamid M, Kelleners-Smeets NWJ. Single versus Multiple Level Sectioning for the Subtyping of Basal-Cell Carcinoma: A Retrospective Study. Dermatology. 2019:1–4.

10. Nori S, Rius-Diaz F, Cuevas J, et al. Sensitivity and specificity of reflectance-mode confocal microscopy for in vivo diagnosis of basal cell carcinoma: a multicenter study. J Am Acad Dermatol. 2004;51(6):923–930. [PubMed: 15583584]

11. Agero AL, Busam KJ, Benvenuto-Andrade C, et al. Reflectance confocal microscopy of pigmented basal cell carcinoma. J Am Acad Dermatol. 2006;54(4):638–643. [PubMed: 16546585]

12. Ulrich M, Roewert-Huber J, Gonzalez S, Rius-Diaz F, Stockfleth E, Kanitakis J. Peritumoral clefting in basal cell carcinoma: correlation of in vivo reflectance confocal microscopy and routine histology. J Cutan Pathol. 2011;38(2):190–195. [PubMed: 21039746]

13. Maier T, Braun-Falco M, Hinz T, Schmid-Wendtner MH, Ruzicka T, Berking C. Morphology of basal cell carcinoma in high definition optical coherence tomography: en-face and slice imaging mode, and comparison with histology. J Eur Acad Dermatol Venereol. 2013;27(1):e97–104. [PubMed: 22540280]

14. Boone MA, Suppa M, Pellacani G, et al. High-definition optical coherence tomography algorithm for discrimination of basal cell carcinoma from clinical BCC imitators and differentiation between common subtypes. J Eur Acad Dermatol Venereol. 2015;29(9):1771–1780. [PubMed: 25712021]

15. Meekings A, Utz S, Ulrich M, et al. Differentiation of Basal Cell Carcinoma Subtypes in Multi-Beam Swept Source Optical Coherence Tomography (MSS-OCT). J Drugs Dermatol. 2016;15(5):545–550. [PubMed: 27168263]

16. Sahu A, Cordova M, Gill M, et al. In vivo identification of amyloid and mucin in basal cell carcinoma (BCC) with combined reflectance confocal microscopy (RCM)- optical coherence tomography (OCT) device and direct histopathological correlation. J Am Acad Dermatol. 2019.

17. Castro RP, Stephens A, Fraga-Braghiroli NA, et al. Accuracy of in vivo confocal microscopy for diagnosis of basal cell carcinoma: a comparative study between handheld and wide-probe confocal imaging. J Eur Acad Dermatol Venereol. 2015;29(6):1164–1169. [PubMed: 25338750]

18. Cinotti E, Jaffelin C, Charriere V, et al. Sensitivity of handheld reflectance confocal microscopy for the diagnosis of basal cell carcinoma: A series of 344 histologically proven lesions. J Am Acad Dermatol. 2015;73(2):319–320. [PubMed: 26183977]

19. Kadouch DJ, Schram ME, Leeflang MM, Limpens J, Spuls PI, de Rie MA. In vivo confocal microscopy of basal cell carcinoma: a systematic review of diagnostic accuracy. J Eur Acad Dermatol Venereol. 2015;29(10):1890–1897. [PubMed: 26290493]

20. Kadouch DJ, Leeflang MM, Elshot YS, et al. Diagnostic accuracy of confocal microscopy imaging vs. punch biopsy for diagnosing and subtyping basal cell carcinoma. J Eur Acad Dermatol Venereol. 2017;31(10):1641–1648. [PubMed: 28370434]

21. Lupu M, Popa IM, Voiculescu VM, Caruntu A, Caruntu C. A Systematic Review and Meta-Analysis of the Accuracy of in VivoReflectance Confocal Microscopy for the Diagnosis of Primary Basal Cell Carcinoma. J Clin Med. 2019;8(9).

22. Mogensen M, Joergensen TM, Nurnberg BM, et al. Assessment of optical coherence tomography imaging in the diagnosis of non-melanoma skin cancer and benign lesions versus normal skin: observer-blinded evaluation by dermatologists and pathologists. Dermatol Surg. 2009;35(6):965–972. [PubMed: 19397661]

23. Ulrich M, von Braunmuehl T, Kurzen H, et al. The sensitivity and specificity of optical coherence tomography for the assisted diagnosis of nonpigmented basal cell carcinoma: an observational study. Br J Dermatol. 2015;173(2):428–435. [PubMed: 25904111]

24. Cheng HM, Lo S, Scolyer R, Meekings A, Carlos G, Guitera P. Accuracy of optical coherence tomography for the diagnosis of superficial basal cell carcinoma: a prospective, consecutive, cohort study of 168 cases. Br J Dermatol. 2016;175(6):1290–1300. [PubMed: 27146027]

25. Sahu A, Yelamos O, Iftimia N, et al. Evaluation of a Combined Reflectance Confocal Microscopy-Optical Coherence Tomography Device for Detection and Depth Assessment of Basal Cell Carcinoma. JAMA Dermatol. 2018;154(10):1175–1183. [PubMed: 30140851]
26. Wang KX, Meekings A, Fluhr JW, et al. Optical coherence tomography-based optimization of mohs micrographic surgery of Basal cell carcinoma: a pilot study. Dermatol Surg. 2013;39(4):627–633. [PubMed: 23293854]
27. Aleissa S, Navarrete-Dechent C, Cordova M, et al. Presurgical evaluation of basal cell carcinoma using combined reflectance confocal microscopy-optical coherence tomography: A prospective study. J Am Acad Dermatol. 2020;82(4):962–968. [PubMed: 31634517]
28. Navarrete-Dechent C, Aleissa S, Cordova M, et al. Management of complex head-and-neck basal cell carcinomas using a combined reflectance confocal microscopy/optical coherence tomography: a descriptive study. Arch Dermatol Res. 2020.
29. Iftimia N, Yelamos O, Chen CJ, et al. Handheld optical coherence tomography-reflectance confocal microscopy probe for detection of basal cell carcinoma and delineation of margins. J Biomed Opt. 2017;22(7):76006. [PubMed: 28697233]
30. Longo C, Lallas A, Kyrgidis A, et al. Classifying distinct basal cell carcinoma subtype by means of dermatoscopy and reflectance confocal microscopy. J Am Acad Dermatol. 2014;71(4):716–724 e711. [PubMed: 24928707]
31. Lupu M, Popa IM, Voiculescu VM, et al. A Retrospective Study of the Diagnostic Accuracy of In Vivo Reflectance Confocal Microscopy for Basal Cell Carcinoma Diagnosis and Subtyping. J Clin Med. 2019;8(4).
32. Themstrup L, De Carvalho N, Nielsen SM, et al. In vivo differentiation of common basal cell carcinoma subtypes by microvascular and structural imaging using dynamic optical coherence tomography. Exp Dermatol. 2018;27(2):156–165. [PubMed: 29215761]
33. Marino ML, Rogers T, Sierra Gil H, Rajadhyaksha M, Cordova MA, Marghoob AA. Improving lesion localization when imaging with handheld reflectance confocal microscope. Skin Res Technol. 2016;22(4):519–520. [PubMed: 26792361]
34. Navarrete-Dechent C, Cordova M, Aleissa S, et al. Use of paper tape to guide reflectance confocal microscopy navigation of large skin lesions. J Am Acad Dermatol. 2019.
35. Navarrete-Dechent C, Mori S, Cordova M, Nehal KS. Reflectance confocal microscopy as a novel tool for presurgical identification of basal cell carcinoma biopsy site. J Am Acad Dermatol. 2019;80(1):e7–e8. [PubMed: 30244067]
36. Pellacani G, Farnetani F, Gonzalez S, et al. In vivo confocal microscopy for detection and grading of dysplastic nevi: a pilot study. J Am Acad Dermatol. 2012;66(3):e109–121. [PubMed: 21742408]
37. Gill M, Longo C, Farnetani F, Cesinaro AM, Gonzalez S, Pellacani G. Non-invasive in vivo dermatopathology: identification of reflectance confocal microscopic correlates to specific histological features seen in melanocytic neoplasms. Journal of the European Academy of Dermatology and Venereology. 2014;28(8):1069–1078. [PubMed: 24147614]
38. Saknite I, Gill M, Alessi-Fox C, et al. Features of cutaneous acute graft-versus-host disease by reflectance confocal microscopy. Br J Dermatol. 2019;181(4):829–831. [PubMed: 30927259]

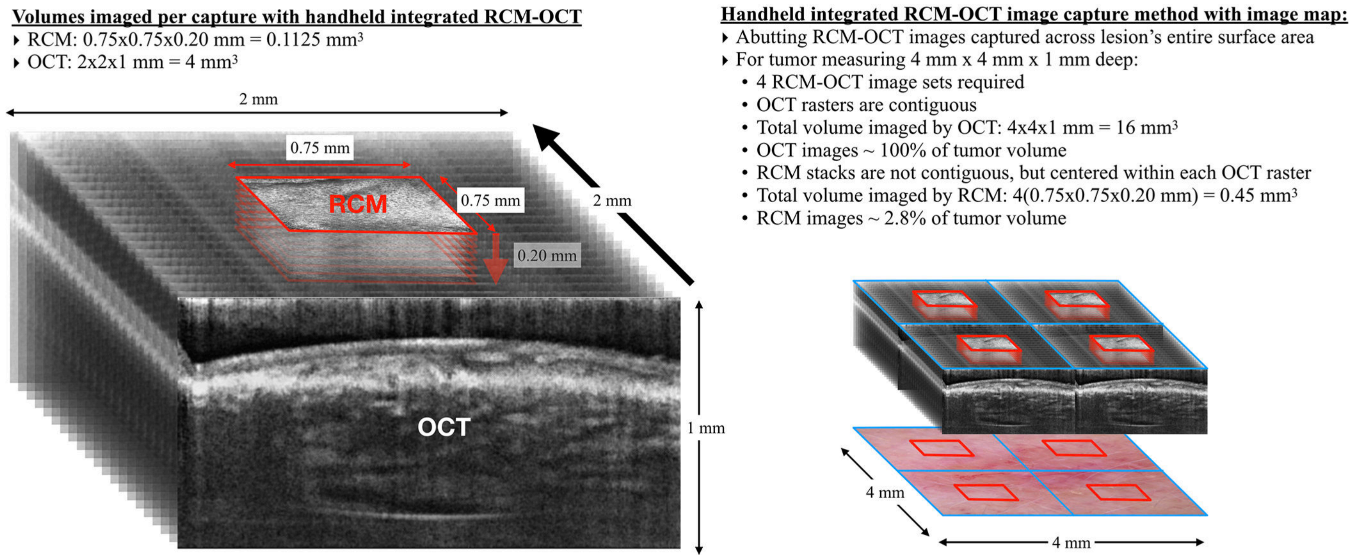

Figure 1. Three-dimensional (3D) volume of skin imaged by the handheld integrated reflectance confocal microscopy-optical coherence tomography (RCM-OCT) device and image capture method used for study protocol.

With the integrated RCM-OCT device, the OCT raster displays a 2 mm × 2 mm by 1 mm deep 3D volume of skin viewed as a video compilation of consecutive moderate resolution (~10 μm) images sequentially captured at regular intervals while moving through the skin in the vertical plane (thick black arrow), analogous on histopathology to leveling through a tissue block of skin embedded on edge. The RCM image stack is captured in the center of the OCT field of view and consists of consecutive 0.75 mm × 0.75 mm horizontal high resolution (~1 μm) images sequentially captured from the surface of the skin to a depth of ~0.20 mm (thick red arrow), analogous on histopathology to leveling through a punch biopsy of skin embedded en face in the setting of alopecia evaluation. Comprehensive evaluation of a lesion's 3D volume by OCT is achieved by acquiring consecutive adjacent RCM-OCT image sets across a lesion's entire surface. Assuming OCT captures 100% of the tumor volume, RCM only captures 2.8% of the tumor volume using this protocol.

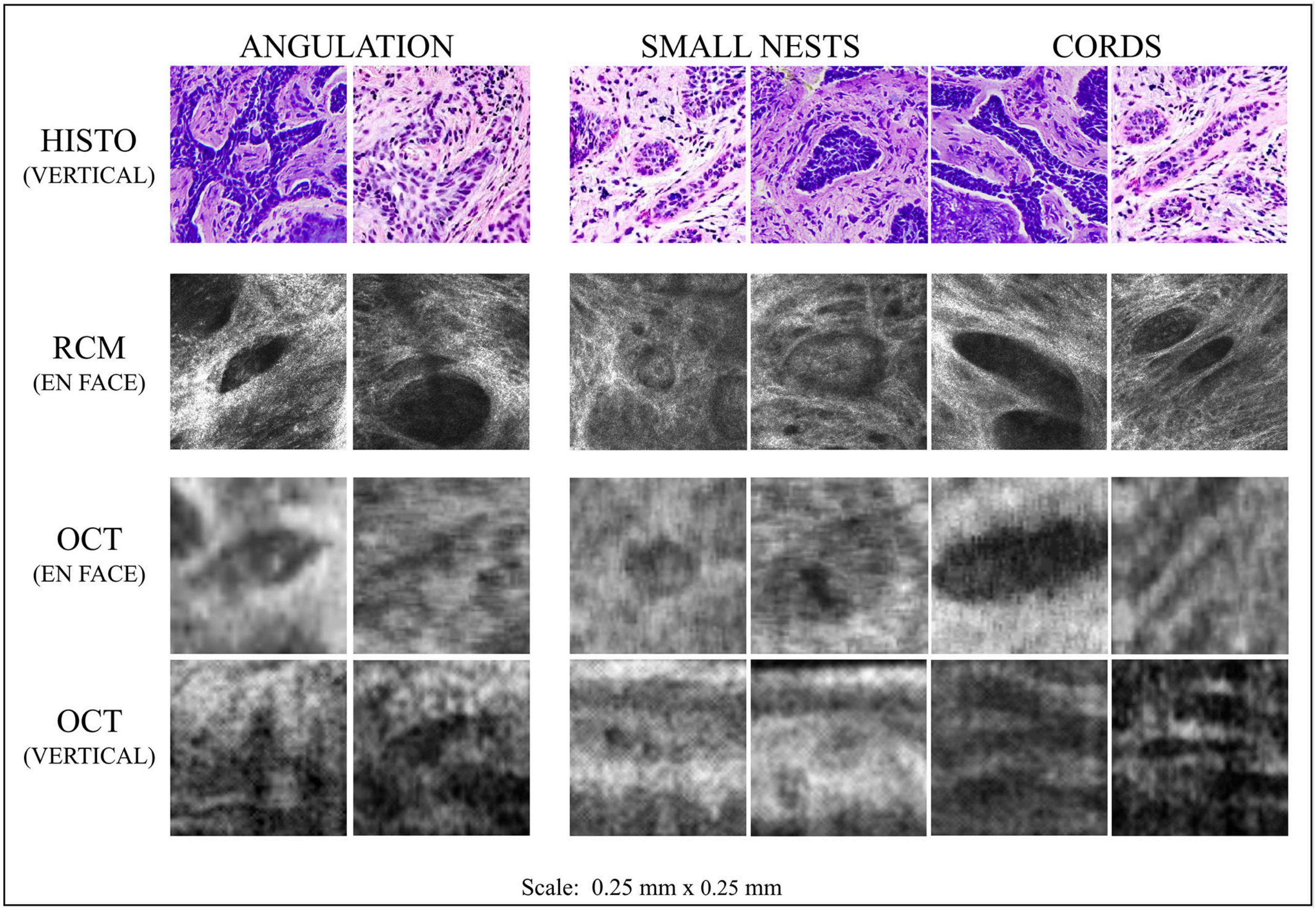

Figure 2. Examples of *angulation, small nests, and cords* across modalities.

Images are shown at identical scale (0.25 mm × 0.25 mm) with feature example centered in each image. Row 1: vertical hematoxylin and eosin (H&E)-stained histopathologic sections. Row 2: en face reflectance confocal microscopy (RCM) images. Row 3: en face optical coherence tomography (OCT) images. Row 4: vertical OCT images. Columns 1 and 2: BCC tumor aggregates (any size or configuration) with *angulation,* also described as jagged contours or pointed ends (rather than rounded or curved contours). Columns 3 and 4: *small nest(s)* of BCC, tumor islands that are rounded/oval or angulated/triangular and can vary in size, but some are expected to be <0.15 mm. Columns 5 and 6: *cord(s)* of BCC, also described as strands or tongues, can be long or short (resembling an elongated oval). Histopathology (color) and RCM (gray scale) images show similar resolution, which is superior to that of OCT images (gray scale). On both RCM and OCT, central tumor aggregates are a similar or relatively darker shade of gray as compared to surrounding tumor stroma.

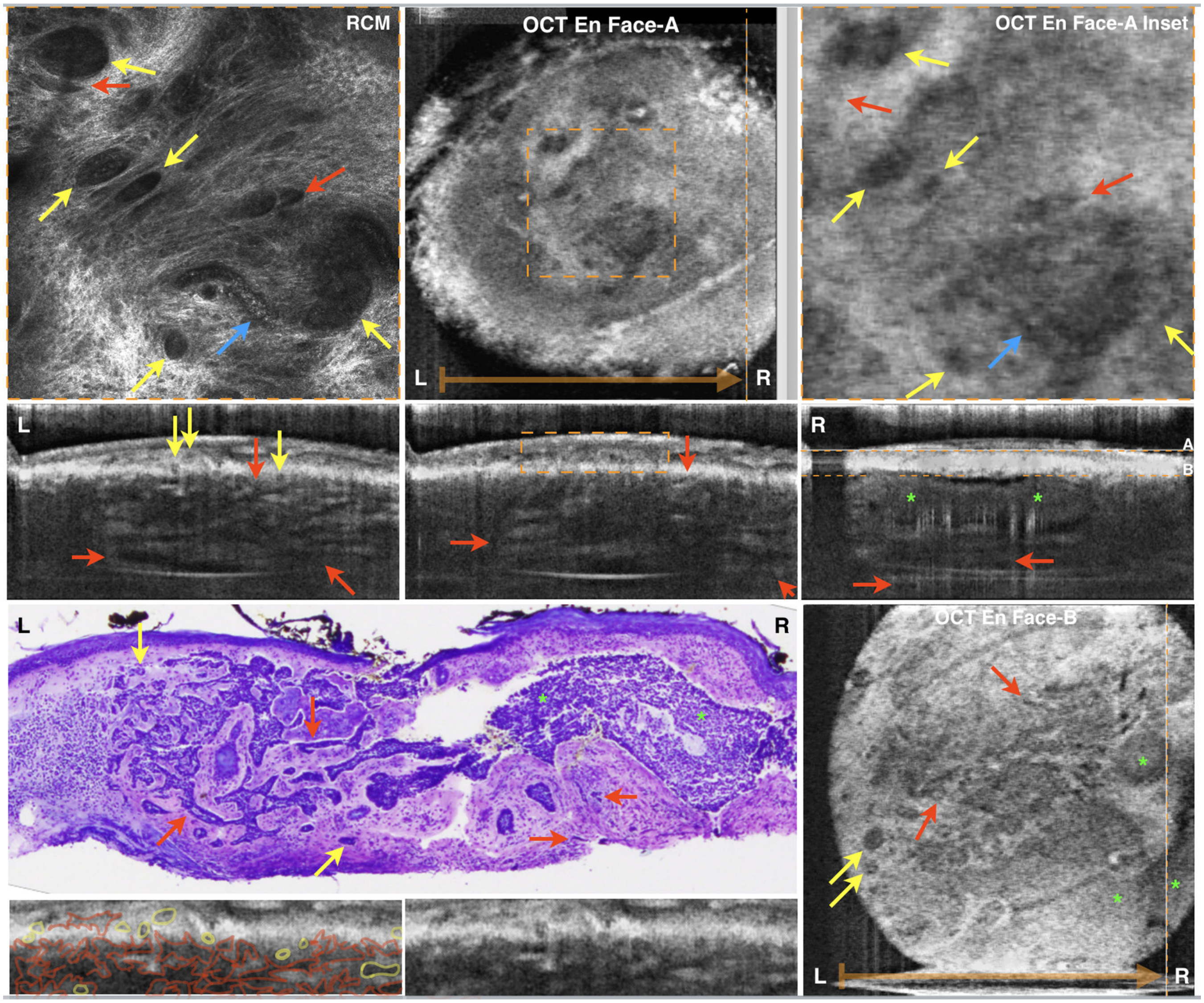

Figure 3. Case 31: BCC, nodulo-infiltrative type on the cheek of a 59 year old woman.
Across all images, red arrows indicate intradermal BCC tumor aggregates with *angulation* and yellow arrows indicate those arranged as *small nests or cords* with rounded contours. OCT en face images (2 mm × 2 mm) are helpful to understand the 3D volume captured by OCT and compare resolutions of OCT and RCM. The area captured by RCM within the center of the OCT raster is indicated by the orange dashed square (0.75 mm × 0.75 mm) and rectangle (0.75 mm × 0.2 mm) in the center of OCT en face-A (row 1) and OCT vertical image (row 2, center), respectively. The vertical dashed orange line on the left of each OCT en face image indicates where the corresponding OCT vertical image (row 2, right) is located; horizontal dashed (A) and interrupted dashed (B) orange lines on OCT vertical image (row 2, right) indicate the depths at which OCT en face images A and B are located. RCM shows individual trafficking leukocytes within a post capillary venule (blue arrow) with much better resolution than OCT; without this registered RCM image, correctly identifying the nature of this structure (blue arrow) on the corresponding lower resolution

OCT en face-A inset at same scale and depth would be challenging. While peripheral palisading of nuclei (dark basaloid nuclei separated by subtle white lines arranged perpendicular to the edge of the tumor) is subtle but discernible in a rounded small BCC nest in the top left corner of the RCM image, only the architecture of tumor aggregates can be visualized on OCT as medium to dark gray shapes within lighter gray stroma. Representative OCT vertical images (2 mm × 1 mm) from left (L), center and right (R) portions of the raster (row 2) are equivalent to low-resolution black and white histopathology sections at 100x magnification. Elongated cords with *angulation* predominate the left and center portions of the lesion on both OCT (L and center, row 2; left and center of en face-B) and histopathology (H&E, 40x magnification). A few round *small nests* are also present. Larger nodule(s) (green asterisks) of BCC dominate the right portion of the lesion on OCT (vertical R and right portion of OCT en face-B) similar to histopathology. The white peritumoral cleft where mucin washed out on histopathology corresponds to the dark peritumoral rim of mucin on OCT. *Small nests and cords* without and with *angulation* are present deep to the large nodular BCC component on both OCT and histopathology. Row 4 shows the upper center of OCT vertical image (L) with and without an overlay showing (manually outlined) contours of tumor aggregates with *angulation* (red) and *small nests and a cord* without *angulation (*yellow).

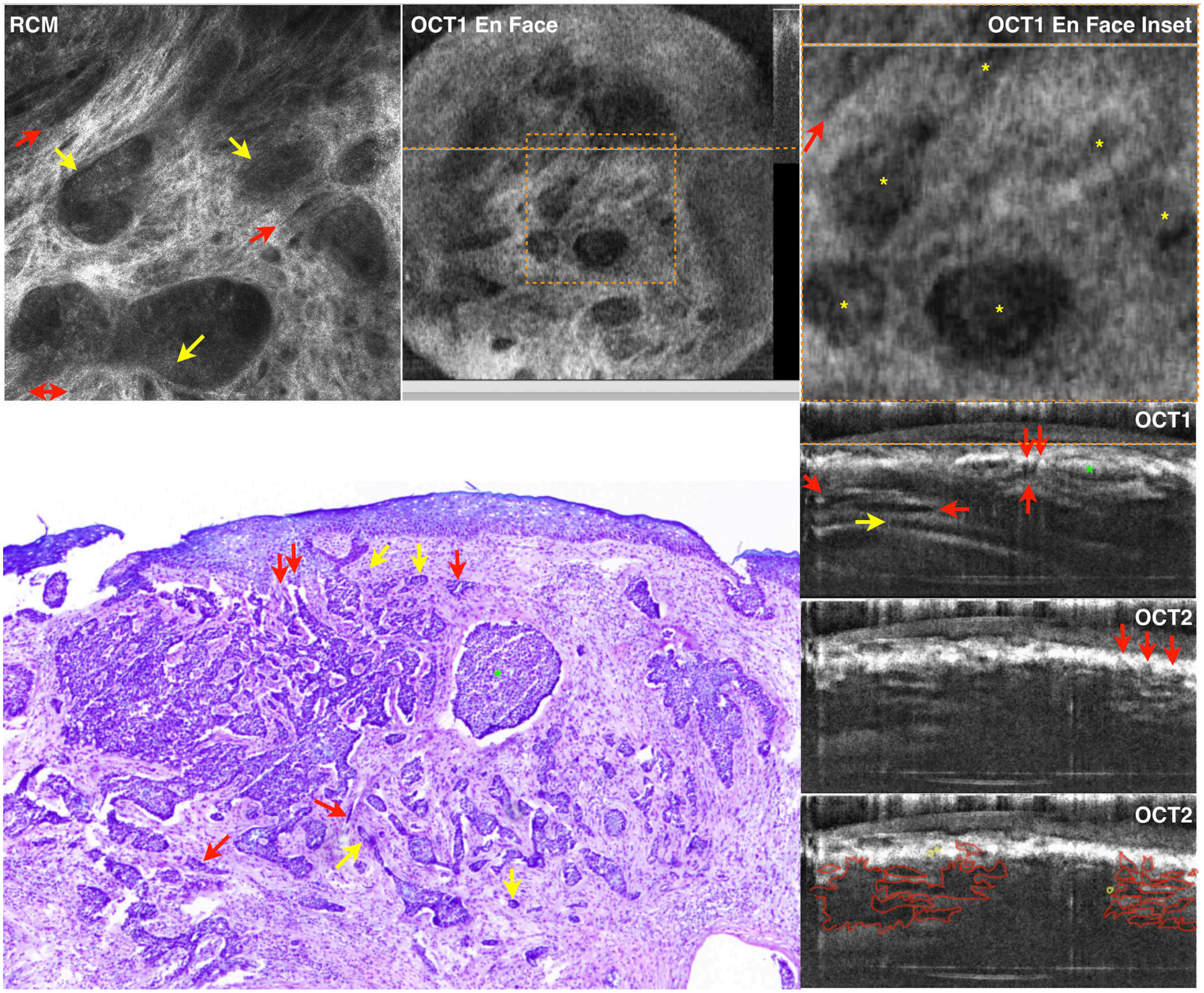

Figure 4. Case 32: BCC, nodulo-infiltrative type, from the left nose of a 93 year old man.
RCM image (0.75 mm × 0.75 mm, top left) shows several *small nests and cords* of BCC, some of which show peripheral palisading of nuclei (yellow arrows). The hook-shaped nest also shows a thin dark rim of mucin (yellow arrow). Red arrows point to tumor *angulation* (pointed ends of some aggregates). The location of the RCM image is within the orange dashed square on the corresponding OCT1 en face image (2 mm × 2 mm) at approximately the same depth (indicated by horizontal orange dashed line on OCT1 vertical image in right column row 2). The OCT1 en face inset shows the corresponding area of the RCM at the same scale (0.75 mm × 0.75 mm), where mostly rounded *small (~0.15 mm - 0.25 mm) nests and a cord* (yellow asterisks) and a cord with *angulation* (red arrow) show much less detail. In the OCT1 vertical image (2 mm × 1 mm) corresponding to the location of the dashed line on OCT1 en face, one can see *angulated cords* of tumor (double red arrows) extending from the epidermis into the dermis in a similar arrangement to histopathology (H&E, 40x magnification). Angulated (red arrows) and rounded (yellow arrow) cords and a larger oval tumor nodule (green asterisk) are also seen. In a vertical image (2 mm × 1 mm) from a

different OCT raster (OCT2), there are several angulated nests and cords (red arrows) on the right side of the image and complex angulated tumor islands and cords in the center and left portion of the image. Several of these structures have been manually outlined in red (indicating those with angulation) and yellow (rounded small nests) on the same OCT2 vertical image in the bottom right corner. Similar structures are present on histopathology.

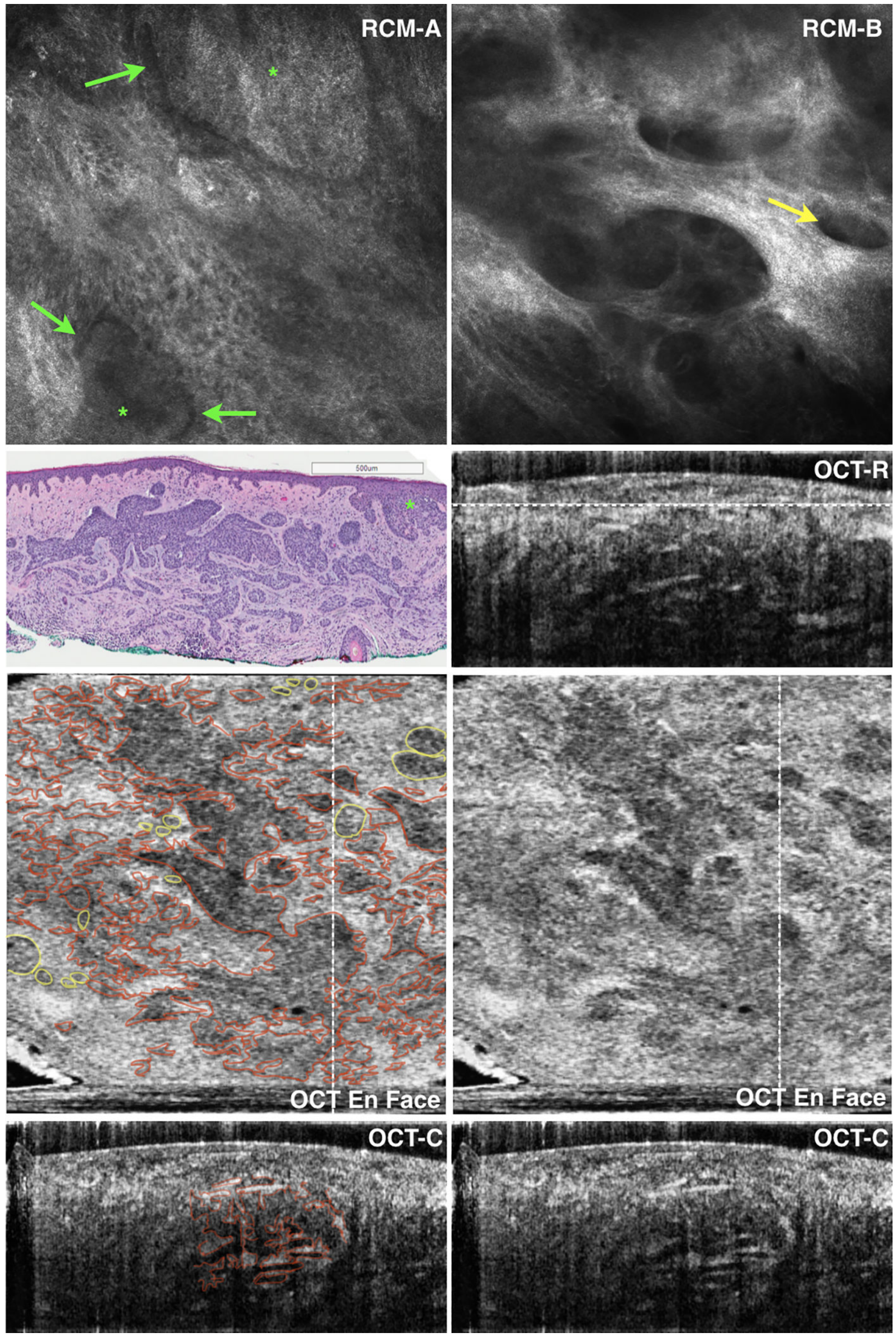

Figure 5. Case 22: BCC, nodulo-infiltrative type, from the forehead of an 83 year old woman.
RCM-A (0.75 mm × 0.75 mm) from just beneath the epidermis shows lobules of BCC (green asterisks) emanating from the undersurface of the epidermis, which are also noted on histopathology (H&E, 100x magnification). Focal subtle peripheral palisading of nuclei and a dark peritumoral rim of mucin are noted (green arrows) on RCM. Deeper in the papillary dermis, a small oval BCC nest (yellow arrow) is noted on RCM-B (0.75 mm × 0.75 mm). Histopathology and OCT-R vertical image (2 mm × 1 mm) viewed at the same scale show similar tumor architecture: dermal tumor aggregates often show *angulation* and some are

arranged as *small nests or cords*. The horizontal dashed white line in vertical OCT-R indicates the depth at which the corresponding OCT en face image is located. The vertical dashed white line in the OCT en face image (2 mm × 2 mm) indicates where the aforementioned OCT-R vertical image is located within the raster (to the right of center). Vertical OCT-C image was captured from the center of the same OCT raster. The bottom 2 rows show duplicate OCT images, one partially (manually) annotated and the other unannotated to highlight aggregates of any size or shape with *angulation* (red) and *small nests* without angulation (yellow).

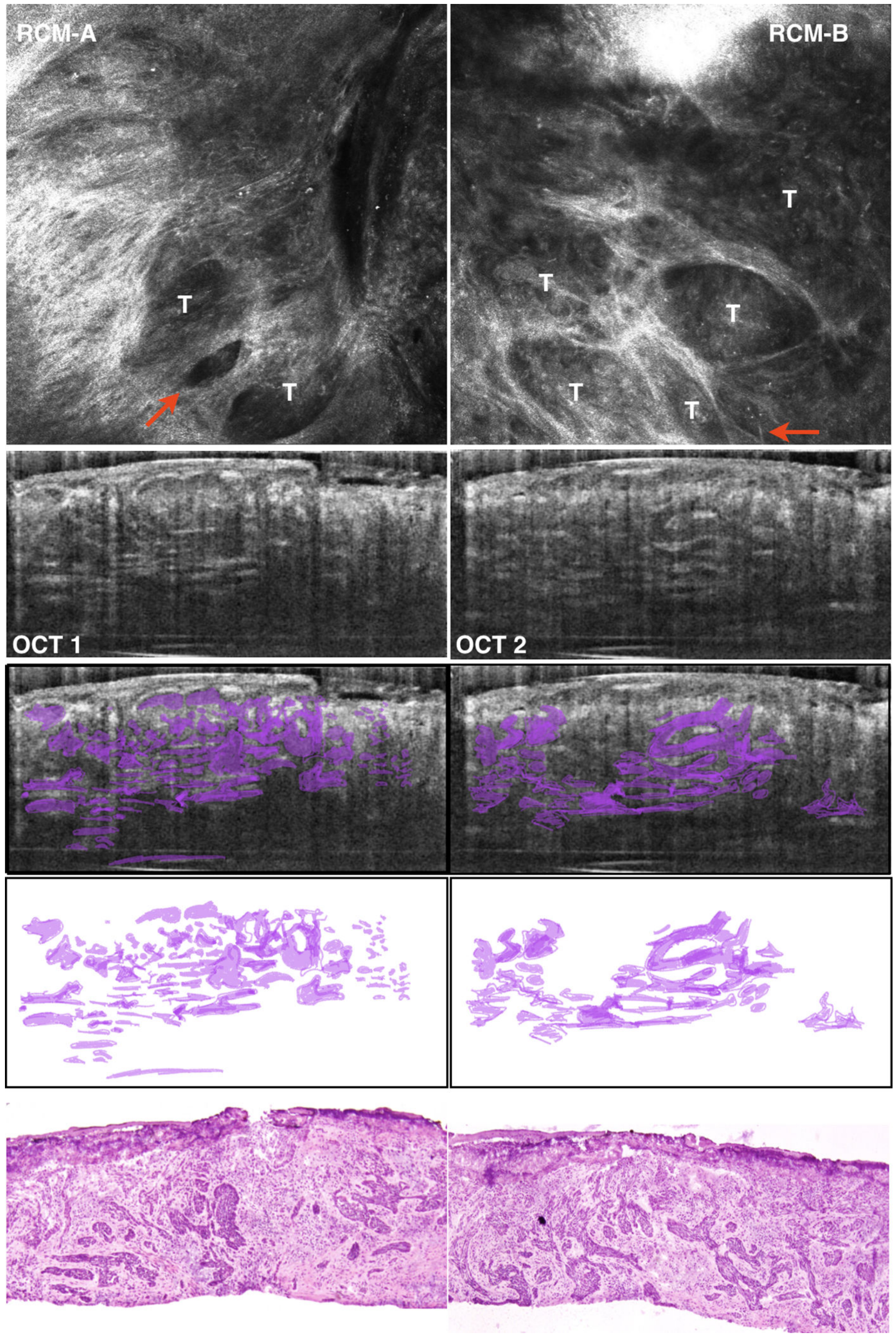

Figure 6. Case 24: BCC, nodulo-infiltrative type, from the forehead of an 85 year old man.
RCM-A&B (0.75 mm × 0.75 mm) in the superficial and deep papillary dermis, respectively, show tumor aggregates (T), some of which are very *small oval nests* with *angulation* (ie end in points, red arrow). Similar to histology (H&E, 100x magnification), tumor nests are composed of larger cells. Only a few nests show peritumoral mucin and none show clear peripheral palisading of nuclei, features commonly absent in infiltrative BCC. In OCT1 and OCT2 vertical images (2 mm × 1 mm), numerous tumor cords, some of which show *angulation*, are noted in the dermis. Row 3 shows the same OCT vertical images with an

Author Manuscript
Author Manuscript
Author Manuscript

overlay in which many of the dark gray dermal tumor aggregates have been manually painted purple. Row 4, represents the overlay from row 3 on a white background to illustrate how the general architecture of the tumor in representative vertical OCT images is similar to that seen in representative histopathology sections (row 5).

Table 1.

Patient demographics and tumor characteristics

Case #	Patient	Age (years)	Gender	Anatomical Location	Histopathological Subtype	Specimen Type (Margins)
BCC Diagnostic Subtype						
Low Risk						
Case 1	Patient 1	66	Male	Left shin	Superficial	Simple excision (margins free)
Case 2	Patient 2	70	Male	Left calf	Superficial	Saucerization (margin free)
Case 3	Patient 2	70	Male	Right shin	Superficial	Saucerization (margin free)
Case 4	Patient 3	63	Female	Right chest	Superficial	Saucerization (margin free)
Case 5	Patient 4	45	Female	Left presternal chest	Superficial-(early) nodular	Saucerization (extending to tissue edge)
Case 6	Patient 4	45	Female	Right upper anterior chest	Superficial-(early) nodular	Saucerization (margin free)
Case 7	Patient 4	45	Female	Left upper anterior chest	Superficial-nodular	Saucerization (margin free)
Case 8	Patient 4	45	Female	Left clavicle	Nodular (early)	Saucerization (margin free)
Case 9	Patient 4	45	Female	Chest	Nodular	Saucerization (margin free)
Case 10	Patient 5	91	Male	Left forearm	Nodular	Saucerization (margin free)
Case 11	Patient 6	63	Male	Left forehead	Nodular	Saucerization (transected)
Case 12	Patient 7	22	Male	Left temple	Nodular	Mohs excision (margins free)
Case 13	Patient 8	59	Male	Right back	Nodular	Saucerization (margin free)
Case 14	Patient 8	59	Male	Right chest	Nodular	Saucerization (margin free)
Case 15	Patient 9	71	Male	Right preauricular	Nodular	Mohs excision (margins free)
Case 16	Patient 10	62	Male	Forehead	Nodular	Mohs excision (margins free)
Case 17	Patient 10	62	Male	Cheek	Nodular	Mohs excision (margins free)
High Risk, Infiltrative Pattern						
Case 18	Patient 11	67	Male	Posterior neck	Superficial-nodulo-infiltrative	Saucerization (transected)
Case 19	Patient 12	83	Female	Left forehead inferior	Superficial-nodulo-infiltrative	Saucerization (NA)
Case 20	Patient 12	83	Female	Left cheek medial	Nodulo-(focally) infiltrative	Saucerization (NA)
Case 21	Patient 12	83	Female	Left cheek lateral	Nodulo-infiltrative	Saucerization (NA)

Case #	Patient	Age (years)	Gender	Anatomical Location	Histopathological Subtype	Specimen Type (Margins)
Case 22	Patient 12	83	Female	Left forehead superior	Nodulo-infiltrative	Saucerization (NA)
Case 23	Patient 13	64	Female	Left cheek	Nodulo-infiltrative	Mohs excision (margins free)
Case 24	Patient 14	85	Male	Left forehead	Nodulo-infiltrative	Mohs excision (margins free)
Case 25	Patient 15	65	Male	Left mandibular cheek	Nodulo-infiltrative	Saucerization (transected)
Case 26	Patient 16	61	Male	Right upper arm	Nodulo-infiltrative	Saucerization (extending to lateral & deep edges)
Case 27	Patient 17	65	Male	Nasal ala	Nodulo-infiltrative	Mohs excision (margins free)
Case 28	Patient 18	83	Male	Right scalp	Nodulo-infiltrative	Mohs excision (margins free)
Case 29	Patient 19	62	Male	Left neck	Nodulo-infiltrative	Saucerization (extending to base)
Case 30	Patient 4	55	Female	Chest	Nodulo-infiltrative	Saucerization (transected at base)
Case 31	Patient 20	59	Female	Right cheek	Nodulo-infiltrative	Mohs excision (margins free)
Case 32	Patient 21	93	Male	Left nose	Nodulo-infiltrative	Mohs excision (margins free)
Case 33	Patient 22	80	Female	Nose	Infiltrative	Saucerization (NA)

Table 2.

Presence of *angulation* and/or *small nests and/or cords* within BCC dermal tumor aggregates on histopathology, integrated RCM-OCT, RCM alone and OCT alone

Case #	**Histology**		**Integrated RCM-OCT**		**RCM**		**OCT**	
BCC Diagnostic Subtype	**Angulation**	**Small Nests and/or Cords**	**Angulation**	**Small Nests and/or Cords**	**Angulation**	**Small Nests and/or Cords**	**Angulation**	**Small Nests and/or Cords**
Low Risk								
Case 1	Absent	Absent	Absent	**Present**	Absent	**Present**	Absent	Absent
Case 2	Absent	Absent	Absent	Absent	Absent	Absent	Absent	Absent
Case 3	Absent	Absent	Absent	Absent	Absent	Absent	Absent	Absent
Case 4	Absent	Absent	Absent	Absent	Absent	Absent	Absent	Absent
Case 5	Absent	Absent	Absent	Absent	Absent	Absent	Absent	Absent
Case 6	Absent	Absent	Absent	Absent	Absent	Absent	Absent	Absent
Case 7	Absent	Absent	Absent	Absent	Absent	Absent	Absent	Absent
Case 8	Absent	Absent	Absent	Absent	Absent	Absent	Absent	Absent
Case 9	Absent	Absent	Absent	Absent	Absent	Absent	Absent	Absent
Case 10	Absent	Absent	**Present**	**Present**	Absent	Absent	**Present**	**Present**
Case 11	Absent	Absent	Absent	Absent	Absent	Absent	Absent	Absent
Case 12	Absent	**Present**	Absent	Absent	Absent	Absent	Absent	Absent
Case 13	Absent	Absent	Absent	Absent	Absent	Absent	Absent	Absent
Case 14	Absent	Absent	Absent	Absent	Absent	Absent	Absent	Absent
Case 15	Absent	Absent	Absent	Absent	Absent	Absent	Absent	Absent
Case 16	**Present**	**Present**	**Present**	**Present**	Absent	Absent	**Present**	**Present**
Case 17	Absent	Absent	Absent	Absent	Absent	Absent	Absent	Absent
High Risk, Infiltrative Pattern								
Case 18	Present	Present	Present	Present	**Absent**	**Absent**	Present	Present
Case 19	Present	Present	Present	Present	Present	Present	Present	Present
Case 20	Present	Present	Present	Present	Present	Present	Present	Present
Case 21	Present	Present	Present	Present	**Absent**	Present	Present	Present
Case 22	Present	Present	Present	Present	**Absent**	Present	Present	Present
Case 23	Present	Present	Present	Present	Present	Present	Present	Present
Case 24	Present	Present	Present	Present	Present	Present	Present	Present
Case 25	Present	Present	Present	Present	**Absent**	**Absent**	Present	Present
Case 26	Present	Present	Present	Present	Present	Present	Present	Present
Case 27	Present	Present	Present	Present	Present	Present	Present	Present
Case 28	Present	Present	Present	Present	**Absent**	**Absent**	Present	Present
Case 29	Present	Present	Present	Present	**Absent**	**Absent**	Present	Present
Case 30	Present	Present	Present	Present	**Absent**	**Absent**	Present	Present

Case #	Histology		Integrated RCM-OCT		RCM		OCT	
BCC Diagnostic Subtype	**Angulation**	**Small Nests and/or Cords**	**Angulation**	**Small Nests and/or Cords**	**Angulation**	**Small Nests and/or Cords**	**Angulation**	**Small Nests and/or Cords**
Case 31	Present	Present	Present	Present	Present	Present	Present	Present
Case 32	Present	Present	Present	Present	Present	Present	Present	Present
Case 33	Present	Present	Present	Present	Present	Present	Present	Present

Author Manuscript

Author Manuscript

Author Manuscript

Table 3.

Sensitivity and specificity of *angulation* and/or *small nests and/or cords* for identifying an infiltrative BCC component across modalities

Feature	Histopathology		Integrated RCM-OCT		RCM		OCT	
	Sensitivity (95% CI)	Specificity (95% CI)	Sensitivity (95% CI)	Specificity (95% CI)	Sensitivity (95% CI)	Specificity (95% CI)	Sensitivity (95% CI)	Specificity (95% CI)
Angulation	100 (79–100)	94 (71–100)	100 (79–100)	88 (64–99)	56 (30–80)	100 (81–100)	100 (79–100)	88 (64–99)
Small Nests and/or Cords	100 (79–100)	88 (64–99)	100 (79–100)	82 (57–96)	69 (41–89)	94 (71–100)	100 (79–100)	88 (64–99)
Angulation *and* Small Nests and/or Cords	100 (79–100)	94 (71–100)	100 (79–100)	88 (64–99)	56 (30–80)	100 (81–100)	100 (79–100)	88 (64–99)

Table 4.

Kappa statistics for the agreement between tumor assessment modalities.

Feature	Histopathology and Integrated RCM-OCT	Histopathology and RCM	Histopathology and OCT
Angulation	0.94	0.52	0.94
Small Nests and/or Cords	0.82	0.53	0.88
Angulation *and* Small Nests and/or Cords	0.94	0.52	0.94

Table 4 interpretation: Histopathology and integrated RCM-OCT as well as histopathology and OCT, which sampled a similar comprehensive volume of tumor per study protocol, exhibit almost perfect agreement for the presence of *angulation* and/or *small nests and/or cords*. Despite the study protocol providing quite limited tumor sampling with RCM, histopathology and RCM achieved moderate agreement for the presence of *angulation* and/or *small nests and/or cords*.